4
Experimentation

4.1 Materials

Table 4.1 shows the elemental analysis of the minerals used for electrode coatings. The elemental analysis of the minerals was conducted using the XRF technique. The elemental composition analysis of the base materials and associated filler wires is shown in Table 4.2.

Table 4.1: Mineral elemental analysis (wt. %)

Mineral (Source)	Ca	Si	Fe	Ti	Al	F	Na	Sr	S	Mg
Calcite (CaO)	82.22	2.95	0.74	-	4.61	-	-	-	-	9.48
Silica (SiO_2)	0.48	96.24	0.17	-	2.82	-	-	-	0.29	-
Fluorspar (CaF_2)	93.24	1.38	0.41	-	4.97	-	-	-	-	-
Rutile (TiO_2)	-	4.09	1.57	88.11	5.94	-	-	-	0.29	-
Cryolite (Na_3AlF_6)	-	0.80	0.002	-	16.17	54.87	28.15	-	-	-
Strontianite (SrO)	0.13	-	0.0009	-	-	-	0.38	97.54	0.12	1.82

Table 4.2: Elemental analysis of filler wire (F) and base metal (BM) (wt.%)

Material	C	Si	Mn	P	S	Cr	Mo	Cu	Fe	Co	Ti	Nb	Ni
IN-617 (BM)	0.06	0.51	0.67	0.01	0.01	22.10	8.20	0.40	1.20	11.52	0.45	0.22	Bal.
SS304H (B)	0.05	0.22	1.08	0.03	0.02	18.05	0.14	0.50	71.22	0.14	-	0.55	8.01
IN-617 (F)	0.04	0.12	0.13	0.01	0.01	21.84	9.10	0.01	0.61	12.10	0.35	-	Bal.

Design and development of nickel-based electrodes for shielded metal arc welding process based on $CaO\text{-}TiO_2\text{-}SiO_2\text{-}Na_3AlF_6$ and $CaO\text{-}CaF_2\text{-}SiO_2\text{-}SrO$ flux system. These two types of flux system are referred as 1st flux system and 2nd flux system for easy readability in the later part of this thesis.

4.2 Design of Experiment (Extreme vertices design)

The coating formulations for welding electrodes were developed using the extreme vertices design approach proposed by previous researchers (Cornell, 2011; McLean and Anderson, 1966). This technique involves a constrained mixture design, the combinations of n constituents with specified upper and lower limits on some or all components, which can be mathematically expressed as follows (Eq.4.1 and Eq. 4.2)

$$0 \le K_i \le y_i \le L_i \le 100 \qquad \text{Eq. (4.1)}$$

$$\sum_{i=1}^{n} y_i = 100 \qquad \text{Eq. (4.2)}$$

Whereas i =1,2,…, n, K_i, and L_i are the higher and lower bounds of restraints on y_i, which is the coating mixture percentage of the primary ingredients. When a mixture has no upper and lower limits on its constituents, defining the geometric features of the constrained design space becomes straightforward. It includes all points situated either on or inside the bounds of a normal simplex with (n-1) dimensions. Consequently, the experimental design space for a n-component mixture is simplified to a (n-1)-dimensional simplex. In a system with three ingredients (n=3), the design space, which is three-dimensional and shaped like

a cube, is simplified to a two-dimensional shape known as a simplex, specifically an equilateral triangle. The design space becomes a tetrahedron form when n = 4, as shown in Figure 4.1. and Figure 4.2.

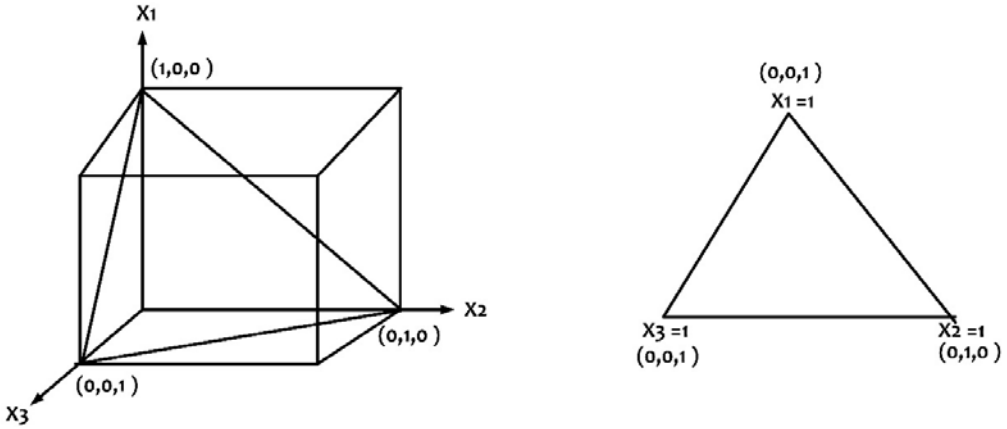

Figure 4.1: Three-component design space (Cornell, 2011)

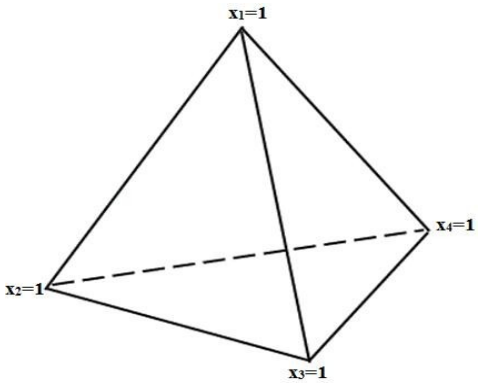

Figure 4.2: Four-component tetrahedron (Cornell, 2011)

Defining the constricted design area is straightforward, even when only a few combination elements are restricted. The combination manifests as a hyper-polyhedron or convex polyhedron when it has more constraints with lower and higher boundaries. Specific design points are determined to represent the relationship between the measured qualities and the constrained mixture design space using Eq. 4.1 and Eq. 4.2. The points in the design space correspond to the different vertices and centroids of the polyhedron's faces. To determine the vertices of a polyhedron, one must first compile a list of all possible proportions for n-1 components, utilizing their lower and upper bound limitations. This may be done using a two-level factorial technique. The amounts of one constituent are unspecified. This approach generates a set of points equal to 2^{n-1}. The identical procedure is iterated for each component, with the amounts of one constituent left blank in the list alternately. The output will consist of a thorough list of $n.2^{n-1}$ viable possibilities. The quantities of the omitted items in the list are stated in a way that meets both their minimum and maximum restrictions while also ensuring that the total amount of all constituents is 100% or unity. Thus, polyhedron vertices are obtained using this approach. The other step is to group the vertices of the polyhedron to get the centroids of its two-dimensional faces. The polyhedron centroid is calculated by averaging the positions of all its vertices. The points in the design space constitute the entire design matrix for experimental purposes. The output responses are observed, and from these observations, the input parameters in the usually mixed-design regression models may be estimated. A second-order regression model may be used to express the output response characteristic of a combination with n constituents as (Eq 4.3):

$$Y = \sum_{i=1}^{n} k_i x_i + \sum_{i<j} \sum^{n} k_{ij} x_i x_j \qquad \text{Eq. (4.3)}$$

In this context, the terms "k_i" and "k_{ij}" refer to the regression coefficients of the least square model. The phrases "$k_i x_i$" and "$k_{ij} x_i x_j$" refer to the individual constituents and their interaction impacts on the different components of electrode coatings, respectively. This type of regression model, known as Scheffe-type models, does not include intercept variables or term x_1^2.

4.3 Design of nickel-based electrode using $CaO\text{-}TiO_2\text{-}SiO_2\text{-}Na_3AlF_6$ flux system

While designing an electrode coating, it is crucial to consider the coating's melting point. In SMAW, the electrode coating has to melt before the base metal and remain molten even after the weld metal has solidified. This information was considered while determining the proportion of the coating composition. As a result, the coating mixture's composite melting temperature should be lower than the melting temperatures of the filler wire and base metal. Figure 4.3 depicts the ternary phase diagram of the $CaO\text{-}TiO_2\text{-}SiO_2$ system, which was utilized to develop electrode coating compositions by identifying points (encircled region). These points were chosen to obtain the slag's lower composite melting point (about 1365°C). The extreme vertices mixture design determines the lower and upper limits of the electrode coating composition of CaO, SiO_2, TiO_2, and Na_3AlF_6. Cryolite is added to improve slag detachability and facilitate the cleanliness of the weld metal surface for nickel-based electrodes. The estimated coating composition was scaled down to 70%. of the total coating mixture. Further, to lower the composite melting point, 15% fluorspar was added, and the remaining essential electrode coating ingredients were incorporated by weight. The composition range of coating ingredients and their sum is shown in Eq. 4.4 and Eq. 4.5.

$$\begin{aligned} &7.5 \le CaO \le 17.5 \\ &05 \le SiO_2 \le 10 \\ &15 \le TiO_2 \le 22.5 \\ &22.5 \le Na_3AlF_6 \le 30 \end{aligned} \qquad \text{Eq. (4.4)}$$

$$\sum_{j=1}^{4} y_j = 70 \qquad \text{Eq. (4.5)}$$

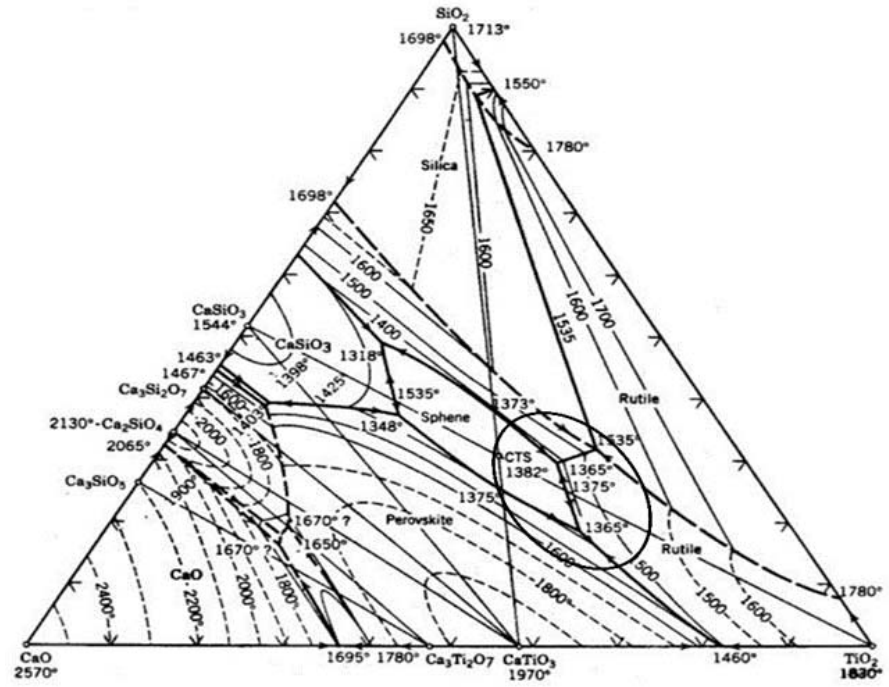

Figure 4.3 Ternary phase diagram of CaO-TiO_2-SiO_2 system (DeVries et al., 1955)

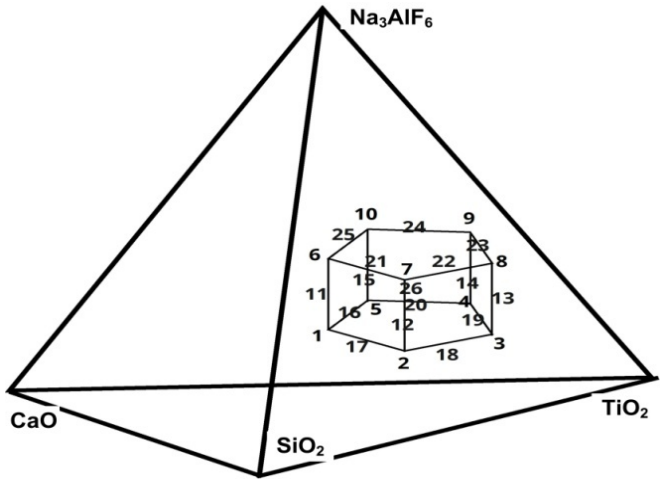

Figure. 4.4 Confined mixture design space

The design matrix for the twenty-six coatings composition formulation was designed using a mixture design methodology, as shown in Table 4.3. Figure 4.4 represents the three-dimensional space diagram for the coating composition. The mixture space diagram comprises fifteen edge centers, one overall centroid, and ten vertices.

Table 4.3: Design matrix for 26 coating composition

#	Flux	Nature of points	Flux Composition				
			CaO	TiO_2	SiO_2	Na_3AlF_6	B.I
1	F1	V	15.0	22.5	5.0	27.5	1.4
2	F2	V	17.5	20.0	5.0	27.5	1.7
3	F3	V	12.5	22.5	5.0	30.0	1.2
4	F4	V	17.5	15.0	8.8	28.8	1.5
5	F5	V	17.5	21.3	8.8	22.5	1.3
6	F6	V	17.5	15.0	10.0	27.5	1.4
7	F7	V	11.3	22.5	10.0	26.3	0.9
8	F8	V	16.3	15.0	10.0	28.8	1.4
9	F9	V	16.3	22.5	8.8	22.5	1.2
10	F10	V	17.5	17.5	5.0	30.0	1.8
11	F11	EC	11.3	18.8	10.0	30.0	1.0
12	F12	EC	17.5	22.5	6.3	23.8	1.4
13	F13	EC	17.5	16.3	6.3	30.0	1.7
14	F14	EC	15.0	22.5	10.0	22.5	1.1
15	F15	EC	16.3	21.3	10.0	22.5	1.2
16	F16	EC	15.0	20.0	5.0	30.0	1.5
17	F17	EC	17.5	22.5	7.5	22.5	1.3
18	F18	EC	17.5	20.0	10.0	22.5	1.3
19	F19	EC	15.5	19.5	8.0	27.0	1.3
20	F20	EC	17.5	15.0	7.5	30.0	1.7
21	F21	EC	7.5	22.5	10.0	30.0	0.7
22	F22	EC	17.5	17.5	10.0	25.0	1.3
23	F23	EC	17.5	22.5	5.0	25.0	1.5
24	F24	EC	10.0	22.5	7.5	30.0	0.9
25	F25	EC	16.3	15.0	8.8	30.0	1.5
26	F26	OC	15.0	15.0	10.0	30.0	1.3

Note: V - Vertex, EC- Edge Centre, OC- Overall Centroid, B.I- Basicity index

4.4 Design of nickel-based electrode using CaO-CaF_2-SiO_2-SrO flux system

In the SMAW process, the composite melting temperature of the coating mixture was less than the melting point of the filler wire. This point was considered while selecting the mixture composition to keep the composite melting temperature of the electrode coating combination well below the limit. The ternary phase diagram of CaO-SiO_2-CaF_2 (Fig.4.5 and Fig 4.6) is used to locate the points corresponding to the lower melting point and their design space diagram. The extreme vertices mixture design determines the lower and upper limits of SiO_2, CaF_2, CaO, and SrO. The higher and lower limits of the coating mixture were selected as 65% of the total coating mixture. The coatings above include 10% potassium silicate as a binder. The remaining 25% was used to add cryolite and rutile to increase weld cleanliness, arc stability, and slag detachability. The composition range of coating ingredients and their sum is shown in Eq. 4.6 and Eq. 4.7. The electrode coating formulation matrix is represented in Table 4.4. The three-dimensional space diagram has a five-plane center, nine-edge centers, six vertices, and one overall centroid.

$15 \le CaO \le 25$
$25 \le CaF_2 \le 35$ Eq. (4.6)
$10 \le SiO_2 \le 15$
$05 \le SrO \le 15$

$$\sum_{i=1}^{4} y_i = 65 \qquad \text{Eq. (4.7)}$$

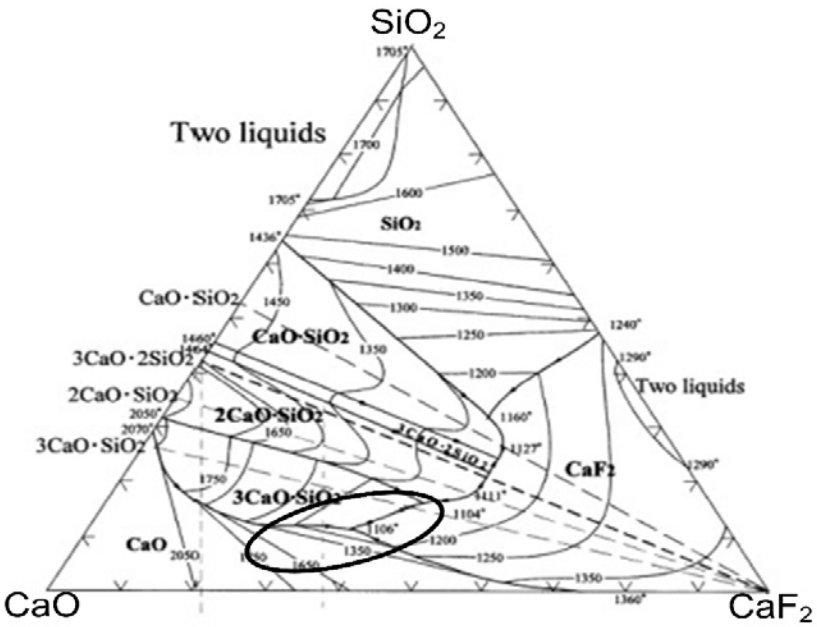

Figure 4.5 Ternary phase diagram of CaO-TiO_2-SiO_2 system (MUKERJI, 1965)

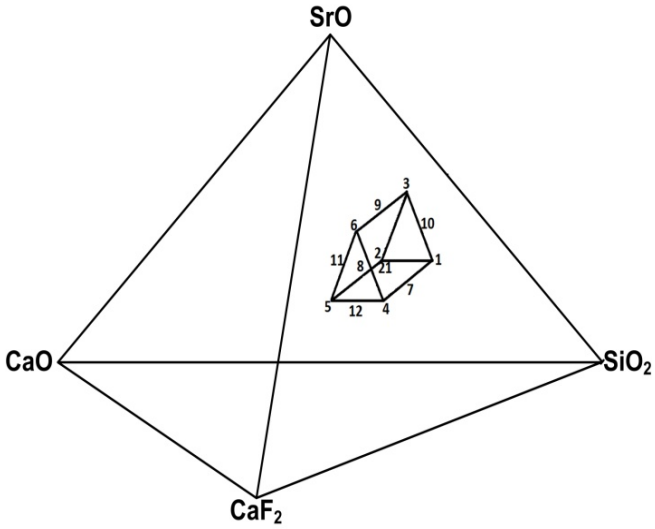

Figure. 4.6 Confined design space diagram

Table 4.4: Electrode coating design matrix

#	Coating	Nature of points	Flux composition				B.I
			CaO	CaF_2	SiO_2	SrO	
1	C1	V	15.0	25.0	15.0	10.0	2.2
2	C2	V	17.5	25.0	15.0	7.5	2.2
3	C3	V	25.0	25.0	10.0	5.0	3.1
4	C4	V	20.0	30.0	10.0	5.0	3.1
5	C5	V	18.3	28.3	10.0	8.3	2.2
6	C6	V	22.5	25.0	12.5	5.0	2.6
7	C7	EC	18.8	28.8	12.5	5.0	2.6
8	C8	EC	15.0	35.0	10.0	5.0	3.1
9	C9	EC	15.0	27.5	15.0	7.5	3.1
10	C10	EC	20.0	25.0	10.0	10.0	3.1
11	C11	EC	15.0	32.5	12.5	5.0	2.6
12	C12	EC	17.5	27.5	12.5	7.5	2.6
13	C13	EC	16.7	26.7	15.0	6.7	2.2
14	C14	EC	15.0	25.0	12.5	12.5	2.6
15	C15	EC	15.0	30.0	15.0	5.0	2.2
16	C16	PC	15.0	30.0	10.0	10.0	3.1
17	C17	PC	15.0	28.8	12.5	8.8	2.6
18	C18	PC	20.0	25.0	15.0	5.0	2.2
19	C19	PC	15.0	25.0	10.0	15.0	3.1
20	C20	PC	17.5	27.5	15.0	5.0	2.2
21	C21	OC	18.8	25.0	12.5	8.0	2.6

Note: V - Vertex, EC- Edge Centre, OC- Overall Centroid, B.I- Basicity index

4.5 Experimentation

4.5.1 Preparation of electrode coating

The individual mineral powders were weighed according to the design matrix and mixed in a hybrid mode comprising manual and equipment-based motorized mixing. Manual mixing was done to ensure no individual mineral powder was left out and that a homogeneous dry mix of powders was obtained. The binder, potassium silicate (K_2SiO_3), and china clay were added to this dry mix to enhance bonding and extrudability. The wet mixture obtained after adding the binder was placed in a motorized mixer at a low-speed range and left for 30 minutes to mix properly. The prepared wet mixture was left for 36 hours to air dry, followed by oven baking for 3 hours at a temperature of 160°C. The air and oven drying eliminated the moisture content from the prepared mixture.

4.5.2 Physicochemical and Thermophysical properties of electrode coatings

The physicochemical and thermophysical properties of the electrode coatings, such as density, thermal conductivity, specific heat, thermal diffusivity, change in enthalpy, thermal stability, and wettability behavior, significantly impact the fabricated welds. Various measurement techniques and experimental setups were employed to examine these properties. The coating mixture was baked, crushed into a fine powder, and verified using a multi-pass grain refinement sieve to perform the characterizations.

4.5.2.1 Density

The density of the coated powder was determined using the bulk density approach. This was done by pouring the powder sample into a measuring cylinder. A weighing scale with an accuracy of ± 0.001 gms was used to measure the quantity of coated powder specimen in a 10 ml measuring cylinder. It is calculated by the ratio of the mass of the coating powder to volume. The average density of each coating mixture was calculated by measuring it three times.

4.5.2.2 Thermal properties (Thermal conductivity, diffusivity, specific heat, change in enthalpy, weight loss)

The simultaneous thermal analyzer (STA) or thermogravimetric analysis (TGA) device was employed to measure the percentage of weight change at high temperatures to determine the thermal stability of electrode coatings. The required tests were conducted using the Perkin Elmer STA 6000, a simultaneous thermal analyzer. The apparatus has a top-loaded furnace with a platinum crucible that can be adjusted to temperatures ranging from 10 °C to 900 °C at scan speeds ranging from 0.2 to 100 °C/min. It can handle samples with a capacity of about 1000 mg. In this study, 10-15 milligrams of coating powder were placed in a platinum crucible, and the controlled thermal scanning was carried out in the temperature range of 25ºC to 900ºC at the rate of 20º/min. The coating's thermal properties, such as conductivity, diffusivity, and specific heat, were measured using a hot disc apparatus. A 3.415 mm Kapton sensor was surrounded by the coating powder from all sides, and subsequent thermal scanning in the controlled environment gave a fair measurement of thermal properties.

4.5.2.3 High-temperature wettability measurements

As per the design matrix presented in Tables 4.3 and 4.4, a 60 g mixture was made for each coating composition. This dry mixture was placed in a mortar and smashed with a pestle for around 15 minutes. The minerals must be thoroughly mixed and crushed for a consistent powder mixture. After the powder was adequately mixed, potassium silicate (binder) was added to produce the wet mixture. This prepared wet mix was placed into a 10 mm diameter die set. A force of 200 kg/cm^2 was given to the integrated die and coating powder system using a hydraulic press. A pellet was obtained with dimensions of a height of 13mm and a diameter of 10 mm. These pellets were placed to air dry for 36 hours, followed by 3 hr of baking in an electric oven heated to 260°C. The wettability of laboratory-developed coatings was studied using a 60x60x4 mm SS304H substrate plate. The experiment was conducted at a temperature of 1150°C. Pellets were placed in the furnace at a temperature of 1150°C for 90 sec in the center of the substrate plate. After that, the melted pellets were removed, and photographs were captured from the top and front sides using a digital camera. The pictures were examined with open-source Image-J software for estimating contact angle and spreading area (Joshi and Chhibber, 2018; Kim et al., 2018). The entire experimentation process schematic is shown in Figure 4.7.

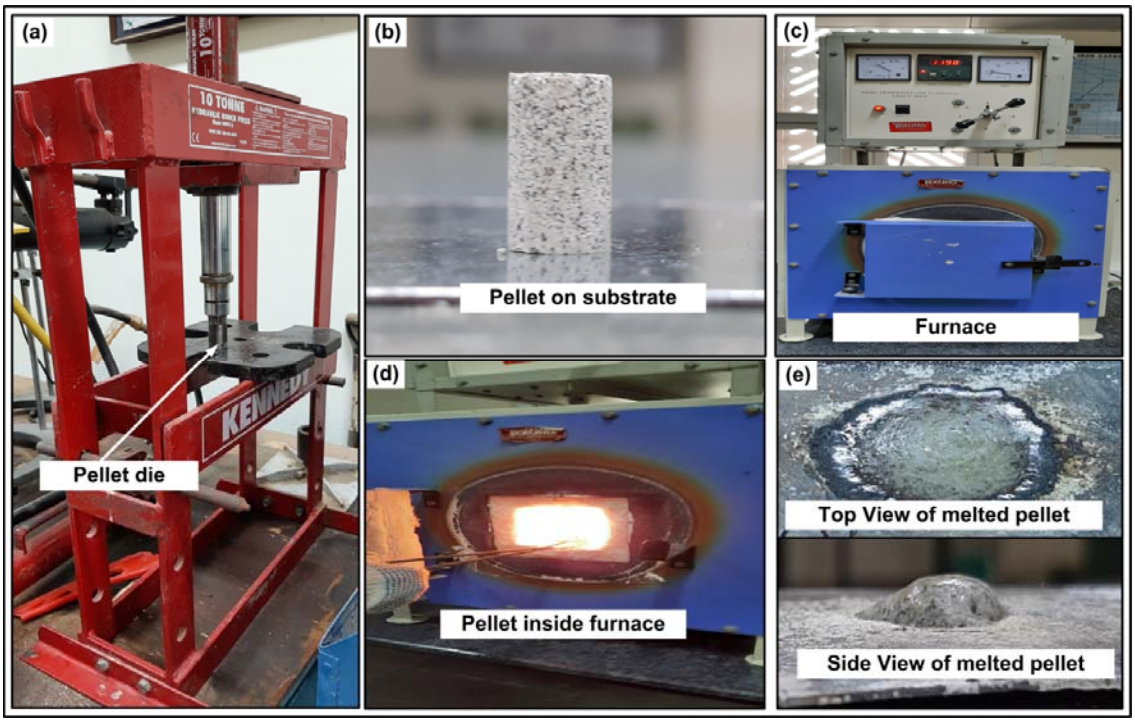

Figure. 4.7: Details of schematic experimental process

The contact angle is an essential parameter for electrode coating flux wettability. The captured image of the melted pellet spread over the substrate determines the contact angle. Image J software measures the angle from both sides of the molten pellet and takes the mean value. At least three measurements were taken for each contact angle to assure repeatability and maintain standard deviation under limits. The contact angle and spreading area of the developed coating are shown in Figure 4.8. The spreading area is one of the important factors in assessing flux performance. Better protection is provided when more slag covers the weld zone. Slag formation during the melting process of coating is used to shield the weld bead from air gases and other impurities. The image captured from the digital camera was analyzed using Image J software. The molten pellets area was marked, and the numerical value of the spread area was obtained as shown in Figure 4.8.

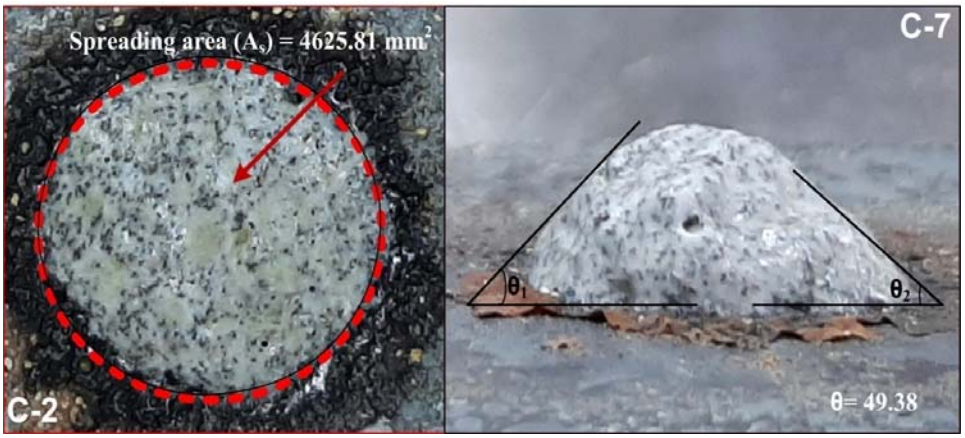

Figure. 4.8: Spreading area of slag and contact angle of molten pellet

After measuring the contact angles for each coating composition, Young's and Boni's equations describe the relationship between the surface and interfacial tensions of different coating at various phase boundaries, such as solid-gas, liquid-gas, or liquid-solid interfaces, based on the observed contact angle findings. Young's equation is represented by Eq. 4.8 and

Figure 4.9 (Hara and Ogino, 1989; Joshi and Chhibber, 2018; Kim et al., 2018; Kingery and Humenik Jr, 1953).

$$\delta_{SG} = \delta_{SL} + \delta_{LG} \cos\theta \qquad \text{Eq. (4.8)}$$

Where θ represents the measured contact angle, δ_{SL} (mN/m) and δ_{SG} (mN/m) are the surface tension at liquid-solid and solid-gas interfaces, and δ_{LG} is the surface tension of melted slag. The surface tension of melted slag (δ_{LG}) was estimated using Boni'sequation, as represented by Eq. 4.9

$$\delta_{LG} = \sum_{k=1}^{n} X_k F_k \qquad \text{Eq. (4.9)}$$

Whereas δ_{LG} is the surface tension of molten slag (mN/m), X_k is the mole % of components k, F_k is the surface tension factor of components. The surface tension factor for different oxides is presented in Table 4.5 (Hara and Ogino, 1989; Joshi and Chhibber, 2018; Kim et al., 2018; Kingery and Humenik Jr, 1953).

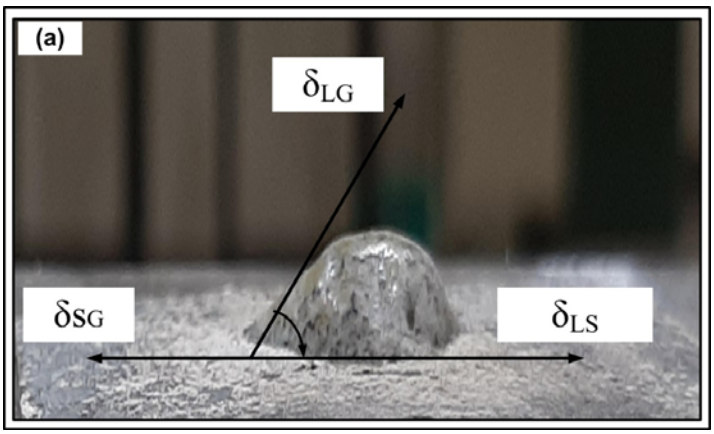

Figure. 4.9: Contact angle and interfacial tensions of molten pellet

Table 4.5: Surface tension factor (F_k) for different oxides

CaO	791-0.0935*T
SiO_2	243.2+0.031*T
CaF_2	407.75-0.07*T
TiO_2	1384.3-0.6254*T
Na_3AlF_6	396.6-0.2*T
SrO	1634.428-0.638*T

Where T is the operating temperature of the furnace. The melting temperature and surface tension factors were used to measure the surface tension values of the developed coating. The adhesion energy is the interfacial property that impacts the wettability behavior of a molten liquid phase with another immiscible phase (W_a). It is inversely proportional to the observed contact angle between solid substrate and liquid metal. The adhesion work is the quantity of energy needed to remove a substance from the substrate. The contact angle should reflect behavior opposite to the adhesion energy because a lower contact angle would increase the interfacial area and resistance between the solid and liquid interface. Adhesion energy is calculated using the equation Dupre-Young and represented by equation 4.10 (Joshi and Chhibber, 2018).

$$W_A = \delta_{LG}(1 + \cos\theta) \qquad \text{Eq. (4.10)}$$

Whereas δ_{LG} is the surface tension of the liquid/gas interface, and θ is the observed contact angle.

4.5.3 Structural Characteristics

Electrode coatings must be structurally analyzed after their design and development. The structural behavior of the electrode coating was analyzed using X-ray diffraction (XRD) and Fourier transformation infrared spectroscopy (FTIR) techniques. It determines the phases and bond types present in the various electrode coatings. FTIR is widely used for measuring vibrational spectra. Infrared radiation interacts with vibrating dipole moments that occur in molecules. The structural behavior of produced coatings was observed using a Bruker FTIR spectrometer (Vertex 70 V). This analysis used a potassium bromide pellet as a reference pellet for absorption spectra for FTIR analysis. The powder specimen of 2 mg was thoroughly mixed with 8 mg of potassium bromide and then placed into a die set of diameter 13 mm. After that, a force of 10N was applied using a hydraulic press. Pellets were formed and scanned at 400-4000 cm^{-1} wavenumber to get the absorption spectra. The graph between the transmittance and wavenumber for various electrode coating samples was plotted. XRD analyses were performed with a scan speed of 0.02 degrees per minute and Cu Kα radiation using a Bruker Powder X-ray diffractometer (PXRD) to determine the various phases in the different electrode coating.

4.5.4 Fabrication of coated electrodes

The fabrication of different welding electrodes, as per Tables 4.3 and 4.4, was done at the pilot plant of an electrode manufacturing company. Figure 4.10 depicts the workings of an electrode manufacturing company. The wet mix was made as per section 4.5.1. A wire feeder was used to hold 350 mm core wires with a diameter of 3.15 mm. The prepared wet mix was fed into a hydraulic press's cylindrical barrel. The electrode coating was extruded onto the IN-617 filler wire using this arrangement. Electrodes were tested to check the eccentricity using a concentric tester. The developed electrodes were evaluated and dried at room temperature for 36 hours before baking at 360°C for 2 hours.



Figure. 4.10: Electrodes manufacturing setup

4.5.5 Selection of Welding Parameters

The welding parameters significantly affect the weld's quality and performance. It is important to fill sufficiently without defects. Welding arcs should be easily ignited and steady, with minimal spatter. Multiple trials were conducted to figure out the final arc current. Various welding currents were used to deposit multipass beads on the base plate while maintaining a constant speed of 2mm/s. The analysis of the bead deposition utilizing IN-617 core wire-based electrodes at various welding currents is presented in Table 4.6. The results showed that a current of 90A increased arc stability, slag detachability, and bead profile.

Table 4.6: Qualitative estimation for bead deposition using developed electrodes

Current (Amp)	Arc stability	Bead appearance	Slag detachability
85	Poor	satisfactory	Poor
90	Good	Good	Good
105	Good	satisfactory	satisfactory
110	Poor	Poor	Poor

4.5.6 Multipass bead on plate experiment

The aim of this experiment to choose the two best electrode coating compositions from the laboratory-developed coating as per Tables 4.3 and 4.4. The fabrication of sets IN-617 electrodes was done, as explained in section 4.5.4. The Shielded metal arc welding (SMAW) setup (Rilon) was used to carry out the bead-on-plate (BOP) experiment, as shown in Figure 4.11. Before welding, a surface grinder was used to clean the base plates. A direct current electrode with positive polarity was used since it promotes high metal deposition. A steady temperature of 150°C to 200°C was maintained between passes. The specimen for examination of weld chemistry, microstructure, and microhardness was prepared by cutting the weld beads to an appropriate length. The samples were polished with silicon carbide emery paper up to 2000 grade and then mirror-polished with cloth. The electro-etching was done using 10 ml of oxalic acid at 9 V for 40 s for the microstructural examination. The chemical composition of the sample was measured using atomic absorption spectroscopy. The Vickers microhardness tester was used to measure the microhardness of each deposited weld. Each specimen had five indentations, and the average value was recorded. Bead appearance, Arc stability, porosity, smoke, slag detachability, and spatter were among the qualitative observations recorded during welding. Chapter 5 discusses the qualitative observations. The two sets of electrodes were chosen from both electrode coating compositions based on qualitative findings, mechanical properties, and weld chemistry to produce the final welds. The final welds were compared to those made with commercial electrodes.

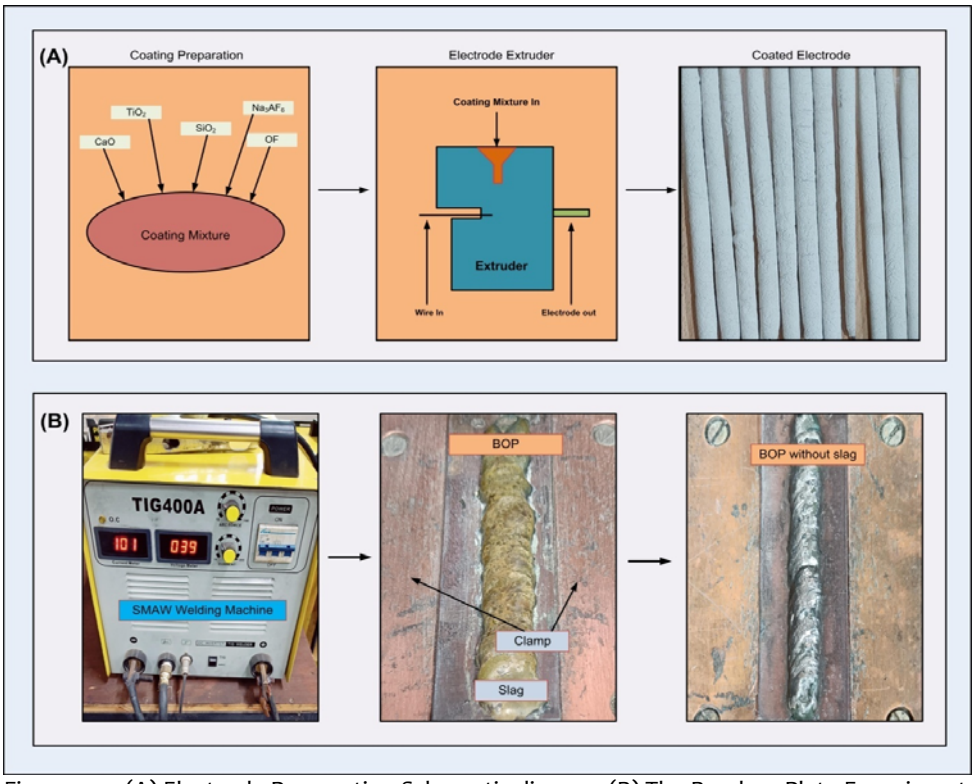

Figure. 4.11 (A) Electrode Preparation Schematic diagram (B) The Bead-on-Plate Experimental Setup

4.5.7 Fabrication of groove design, weld coupons, and dissimilar metal joints

4.5.7.1 Dissimilar metal joints between IN-617 and SS304H utilizing both commercial and developed electrodes

The dissimilar welds were fabricated by cutting the plates from IN-617 and SS304H base materials. The dimensions of the plates were 150 x 60 x 10 mm, and their edges were machined for a groove angle of 30° mm for each plate. The SMAW procedure was used to fabricate three distinct welds of IN-617/SS304H utilizing commercial and two sets of laboratory-developed electrodes. Fabrication of the dissimilar welds was carried out using the parameters listed in Table 4.7. The GTAW process was used for the first tacking of the base plates. The root pass was done using a filler similar to the electrode core wire of diameter 2.4 with the GTAW process. Before the SMAW filling, the tracked plates were preheated to 350°C. SMAW filling was done using direct current electrode positive (DCEP) polarity. Figure 4.12 shows the groove and the final dissimilar weld.

Table 4.7: Welding parameters for dissimilar welds

Welding Parameter	Current (A)	Voltage (V)	Speed (mm/sec)	Argon Gas flowrate (L/min)	Polarity
IN617/SS304H GTAW (Root pass)	100	17.2	1	12	DCEN
IN617/SS304H SMAW (Fill)	90	25	2	-	DCEP

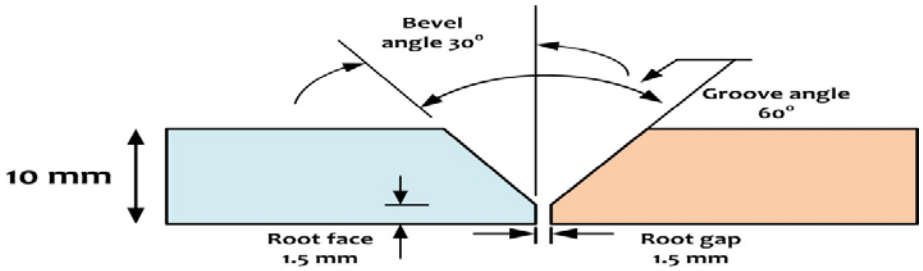

(a)



(b)

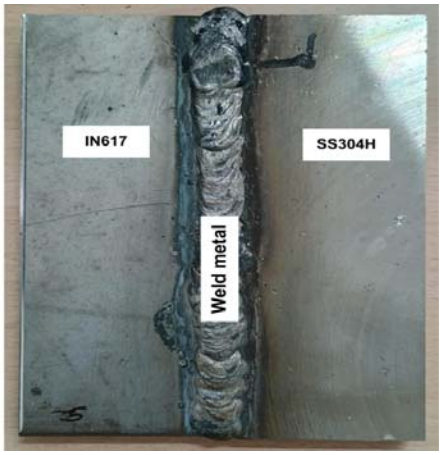

(c)

Figure. 4.12 (a-b) Schematic diagram of conventional V-groove design (c) Top view of welded plate

4.5.7.2 Characterization of fabricated weld

The weld performance was evaluated by analyzing the different characterizations of the fabricated dissimilar welds. The specimen were extracted from the IN617/SS304H DWJ for the metallographic, mechanical (impact, tensile, and microhardness), and corrosion investigation in the transverse direction using a wire-cut electric discharge machine (WCEDM), as seen in Figure 4.13. The ASTM E-8 standard was followed for conducting tensile testing of weld specimens. A 100kN capacity Shimadzu-AG universal testing machine (UTM) was used to perform the tensile test at room temperature on subsize specimens at a 1 mm/min loading rate. The ASTM E-23 standard was followed to assess the impact toughness of weld specimens. The specimens with dimensions 55 mm × 10 mm × 7.5 mm were made for the Charpy test to determine the impact toughness of dissimilar welds. The specimens with notch situated at the weld center were prepared. Three samples were examined for each set of parameters to verify the accuracy of the tensile test and impact toughness test findings. The Vickers microhardness tester determined the microhardness profile of base metal and welded samples using a 500 g load for 10 s dwell time. Spectroscopy was used to assess the chemical compositions of the produced welds. Analysis of the base metal, heat-affected zone, and weld zone microstructures was accomplished by preparing metallographic samples of the weld joint. The samples were polished to a mirror finish using a series of grades of silicon carbide paper: 80, 120, 220, 340, 400, 600, 800, 1000, 1500, and 2000, followed by cloth polishing using alumina paste. Figure 4.13 shows the schematic of the extracted specimen for macro and microstructure examination, mechanical examination (microhardness, tensile, and Charpy test), and corrosion examination. Table 4.8 shows the different etchants utilized to investigate the microstructure of fabricated

dissimilar welds. SEM/EDS was used to analyze fractured tensile and impact toughness specimens.

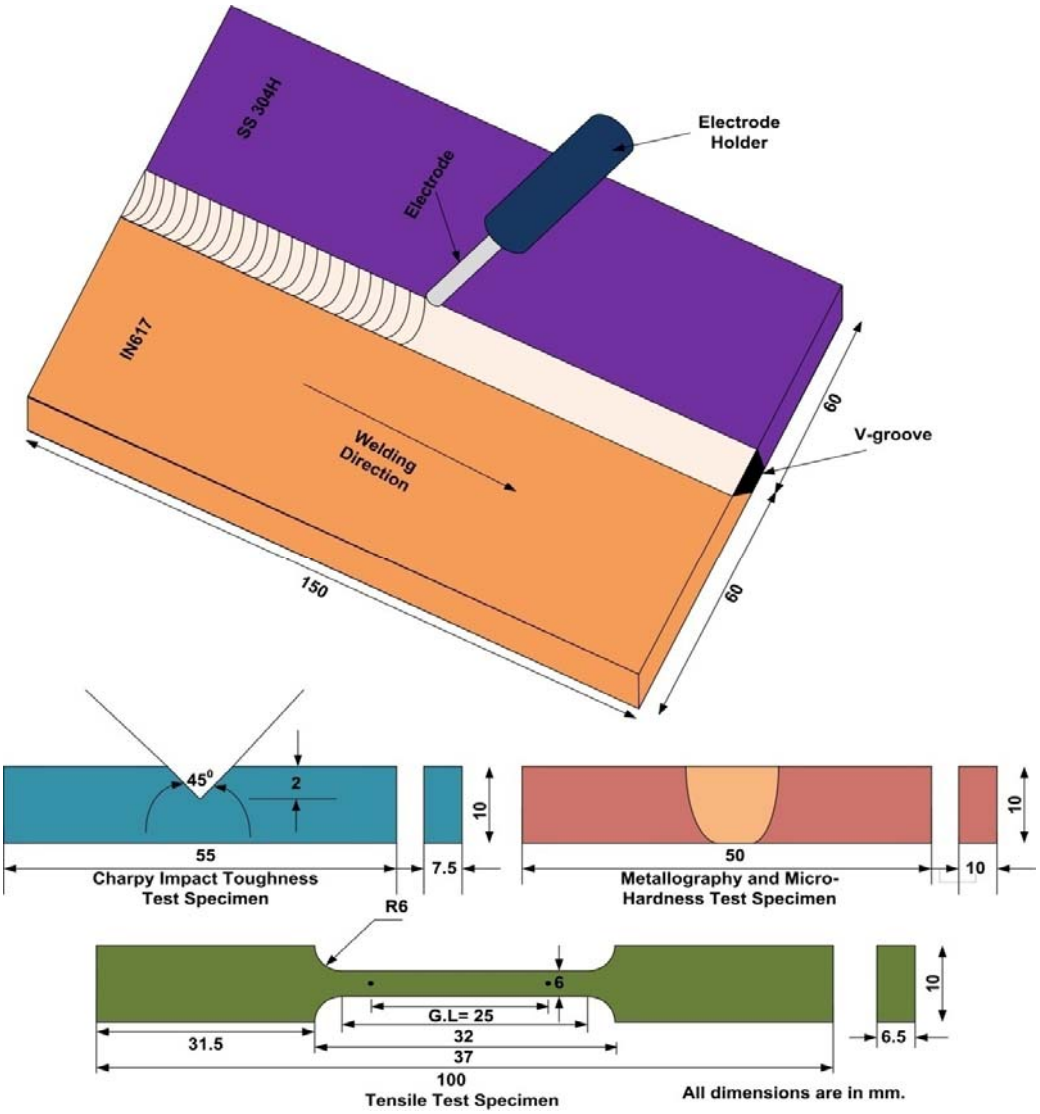

Figure 4.13: Schematic of the extracted specimen for macro and microstructure examination, mechanical examination, and corrosion analysis.

Table 4.8: Etchants used for microstructure analysis of specimens

Etchant	Methods/parameters	Composition	Application area
Aqua Regia	Swab method	15ml HCl + 5ml HNO_3	SS304H base metal and interface
Electrolytically etching (10% oxalic acid)	voltage 9V, current density1A/cm2, time40- 60 sec	10g oxalic acid, 100ml distilled water	IN-617 base metal, interface, and ERNiCrCoMo-1 weld zone

4.5.8 Hot corrosion studies

Hot corrosion experiments were performed on the base materials (IN-617, SS304H) and the welded specimen. The investigations were performed at a temperature of 850°C under the exposure of 75% Na_2SO_4 + 25% NaCl (SM-1) and 75% Na_2SO_4 + 20% NaCl + 5% V_2O_5 (SM-2). The sample was made using wire-cut EDM with dimensions of 20 mm × 10 mm × 5 mm. The samples were polished to a mirror finish using a series of grades of silicon carbide paper: 220, 340, 400, 600, 800, 1000, and 1500, followed by cloth polishing using alumina paste. The dimensions of the polished samples were recorded using the digital vernier caliper to determine surface area. The sample was subjected to an oven at a temperature of 250 °C for one hour in the alumina boat to eliminate any remaining moisture and contaminants. The specified proportion of salt was mixed with distilled water to prepare a thick salt mixture. After an hour, the samples were removed, and a camel brush was used to apply the prepared salt paste to all six faces of the heated sample. The salt mixture was applied to the samples with a 3-5 mg/cm² weight once before starting the corrosion test. After that, the sample was dried in an oven set at 120 °C for three hours to dissipate any remaining moisture. Once the sample had cooled to a normal temperature after three hours in the oven, the weight was recorded along with the alumina crucible, and the initial sample weight was considered. The muffle furnace was adjusted to the proper temperature, and the sample was placed inside for 50 cycles of hot corrosion testing. Every cycle consists of 1 hour of heating at the required temperature and 20 minutes of cooling to room temperature. Weight changes along with the crucible were recorded using an electronic weighing balance with an accuracy of 0.01mg after each cycle. Spalled scales are also taken into consideration during weight measurements. Each experiment was performed in three different samples for all the environments, and the average value of weight gain was taken. The sample was visually observed to illustrate the changes in the oxide scale after each cyclic test. The XRD examination was performed on the corroded samples to analyze the various oxide phases. An energy dispersive spectrometer (EDS) and a scanning electron microscope were used to study the oxide scales' surface morphology and elemental analysis. SEM/EDS elemental point analysis and line scans were employed to examine the cross-section of the samples.